The microwave spectrum of the difluorocyanomethyl radical, ĊF2CN

Lu Kang, Ha Vinh Lam Nguyen, Christopher Falls, Alexander Seys, Wallace Pringle, Thomas Blake, Stewart Novick, S.A. Cooke

▶ **To cite this version:**

Lu Kang, Ha Vinh Lam Nguyen, Christopher Falls, Alexander Seys, Wallace Pringle, et al.. The microwave spectrum of the difluorocyanomethyl radical, ĊF2CN. Journal of Molecular Spectroscopy, 2022, pp.111618. 10.1016/j.jms.2022.111618 . hal-03631719

HAL Id: hal-03631719
https://hal.u-pec.fr/hal-03631719

Submitted on 5 Apr 2022

HAL is a multi-disciplinary open access archive for the deposit and dissemination of scientific research documents, whether they are published or not. The documents may come from teaching and research institutions in France or abroad, or from public or private research centers.

L'archive ouverte pluridisciplinaire **HAL**, est destinée au dépôt et à la diffusion de documents scientifiques de niveau recherche, publiés ou non, émanant des établissements d'enseignement et de recherche français ou étrangers, des laboratoires publics ou privés.

The microwave spectrum of the difluorocyanomethyl radical, $\dot{C}F_2CN$

Lu Kang,[a] Ha Vinh Lam Nguyen,[b,c*] Christopher B. Falls,[d] Alexander B. Seys,[d] Wallace C. Pringle,[d] Thomas A. Blake,[e] Stewart E. Novick,[d] S. A. Cooke[f]

[a] Department of Chemistry and Biochemistry, Kennesaw State University, Kennesaw, GA 30144, United States

[b] Univ Paris Est Creteil and Université Paris Cité, CNRS, LISA, F-94010 Créteil, France

[c] Institut Universitaire de France (IUF), F-75231 Paris, France

[d] Department of Chemistry, Wesleyan University, Hall-Atwater Laboratories, 52 Lawn Ave, Middletown, CT 06459, United States

[e] Pacific Northwest National Laboratory, 902 Battelle Blvd, Richland, WA 99354, United States

[f] School of Natural and Social Sciences, Purchase College SUNY, 735 Anderson Hill Rd, Purchase, NY 10577, United States

*Corresponding author. Email: lam.nguyen@lisa.ipsl.fr

Abstract

The pure rotational spectrum of the open shell difluorocyanomethyl radical, $\dot{C}F_2CN$, has been measured using two Balle-Flygare-type cavity Fourier-Transform-Microwave (FTMW) spectrometers both equipped with pulsed discharged nozzles. A total of 156 transitions (from **N** = 1 – 0 to 6 – 5, and K_a = 0, 1, 2, 3) in the electronic ground state were observed between 6.5 GHz and 38.4 GHz with a typical linewidth of ~5 kHz full-width-half-maximum. A Hamiltonian that included semi-rigid rotor, spin-rotation, and nuclear hyperfine parameters was fit to the observed data set and these parameters have been interpreted and compared to similar radicals. Excellent agreement between experimental and uB3LYP/aug-cc-pVQZ calculated rotational constants, the experimental inertial defect, −0.6858(2) uÅ^2, and the failure of a coupling scheme in which the fluorine nuclei are treated as identical and related by a C_{2v} symmetry axis combine to indicate a nonplanar structure for the $\dot{C}F_2CN$ radical.

Keywords: Microwave spectroscopy, rotational spectroscopy, spin-rotation coupling, nuclear quadrupole coupling, Fermi contact, difluorocyanomethyl radical

Graphical Abstract

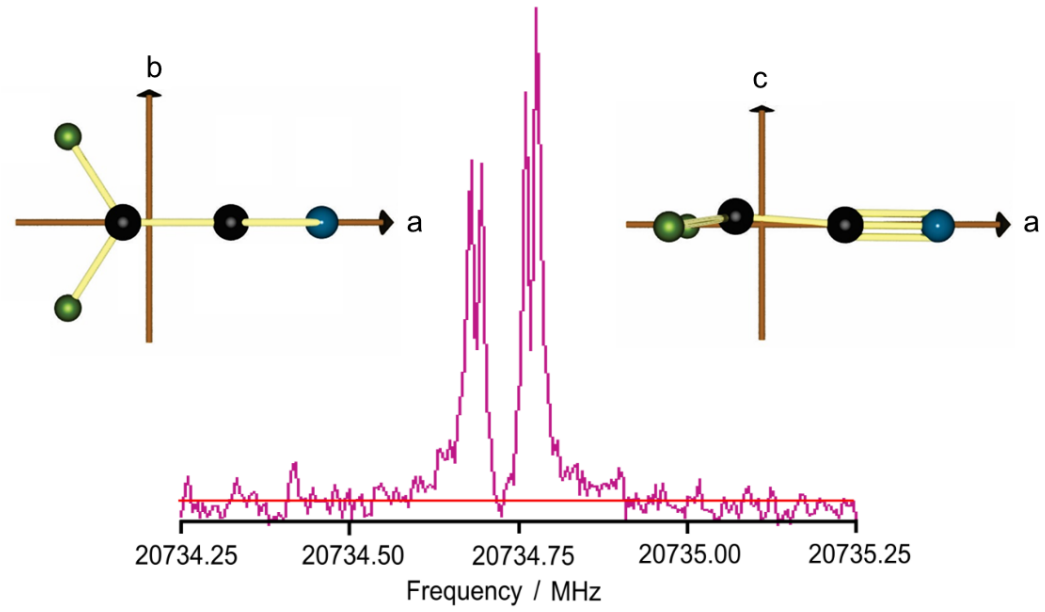

1. Introduction

The methyl radical is known from experiment to be planar [1–4]. However, there is a progression towards a trigonal pyramidal structure as the methyl radical is successively fluorinated, that is, $\dot{C}H_2F$ through $\dot{C}HF_2$ to $\dot{C}F_3$ [5–8], see Figure 1. Theoretical studies have indicated that the planar to pyramidal structural change is due to the increased electronegativity of F over H and the distinct ability of the lone pairs on fluorine to conjugate with the singly occupied carbon atomic orbital [9–11]. In short, the hybridization of the carbon atom progresses from sp^2 in $\dot{C}H_3$ to sp^3 in $\dot{C}F_3$.

But what of other members of the $\dot{C}X_3$ radical family? High resolution spectroscopic studies have been performed on the $\dot{C}H_2X$ subset (X = F, Cl, Br, and I) [12–18], demonstrating that each of these radicals is planar or very close to it. The $\dot{C}H_2X$ subset may be extended by allowing X to be a group of atoms. From this perspective it is of note that both $\dot{C}H_2CCH$ and the isoelectronic $\dot{C}H_2CN$ have also been found to be planar [19,20].

Alongside the development of a coherent structural story of the class of compounds starting from $\dot{C}H_3$ and moving toward $\dot{C}F_3$, it is interesting to consider reversing the direction and studying $\dot{C}F_2X$ radicals. Given that the $\dot{C}H_2X$ radicals are planar; that is, they appear closer to $\dot{C}H_3$ in geometric structure, and one might anticipate that the $\dot{C}F_2X$ radicals would be pyramidal, appearing closer to $\dot{C}F_3$ in geometric structure. However, it is not that straightforward. In 2006, Kang and Novick recorded the microwave spectrum of $\dot{C}F_2CCH$ and determined its structure to be planar [21]. The question on the structure of the isoelectronic radical $\dot{C}F_2CN$ becomes interesting. Will it be planar like $\dot{C}F_2CCH$? Or, recalling that the –CN group is considered a pseudohalogen [22], will it be pyramidal like the $\dot{C}HF_2$ or $\dot{C}F_3$ radicals? We aim to find the answer to this question with the combination of FTMW spectroscopy and quantum chemical calculations.

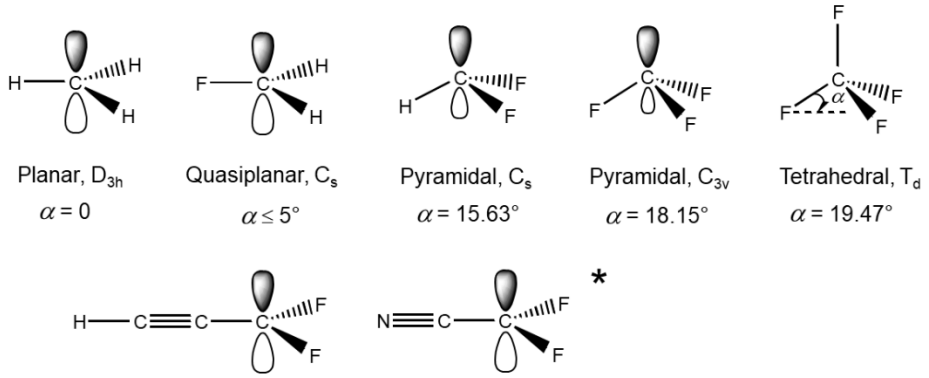

Figure 1. Upper trace: structures of the $\dot{C}H_3$, $\dot{C}FH_2$, $\dot{C}F_2H$, $\dot{C}F_3$ radicals and CF_4 molecule. Lower trace: $\dot{C}F_2CCH$ and $\dot{C}F_2CN$. The star indicates that the planarity of $\dot{C}F_2CN$ is in question. The umbrella angle, α, is defined as $\angle$(C, C, F, F) for the $\dot{C}F_2CCH$ and $\dot{C}F_2CN$ radicals.

Beyond the structural aspects, further motivation arises from environmental concerns [23,24]. Hydrofluorocarbons and perfluorocarbons are greenhouse gases which make contributions to global warming. Many heavy halogenated fluorocarbons such as bromofluorocarbons and chlorofluorocarbons are ozone-depleting substances, which have destroyed the ozone layer for decades. Almost all halocarbons degrade in the atmosphere. For example, $\dot{C}F_2Cl$ and $\dot{C}F_2Br$ are intermediate products of the UVB photodissociation of CF_2Cl_2 (Freon-12, refrigerant, and aerosol spray propellent) and CF_2BrCl (Freon-12B1 or Halon-1211, fire extinguisher). With increasing production due to industrial demands [25,26], effects on environmental change deserve more attention. Hydrogen cyanide is the most common cyanide occurring in the earth's atmosphere with a primary source being biomass burning [27,28]. However, the subsequent degradation mechanisms involving the halogenated alkyl radicals, including the interplay with cyanides, are not well established, largely due to a "lack of laboratory-based information" [29]. The present work provides fundamental spectroscopic constants for the $\dot{C}F_2CN$ radical.

2. Methodology

2.1. Quantum Chemical Calculations

Levchenko and Krylov [30] have pointed out that DFT/uB3LYP [31,32] predictions agree with benchmark studies of the equilibrium properties of many doublet radicals [33–35]. Therefore, the DFT/uB3LYP method was first used in this work for geometry optimizations. All

calculations were performed with the *Gaussian* program [36,37]. We first optimized the geometry at the uB3LYP/aug-cc-pVQZ level of theory to access theoretical equilibrium rotational constants to aid the spectral assignment. Previous studies on other radicals in the literature reported that their molecular structures are not always planar (see Section 1). Therefore, we started with a non-planar geometry for $\dot{C}F_2CN$. The optimized geometry remained non-planar and is illustrated in Figure 2. The Cartesian coordinates are given in Table S-1 in the Supplementary Material. Anharmonic frequency calculations were also carried out at the uB3LYP/aug-cc-pVQZ level to access ground state rotational constants and centrifugal distortion constants. From the calculated dipole moment components of μ_a = 2.11 D, μ_b = 0.00 D, and μ_c = 0.16 D, only *a*-type transitions were expected.

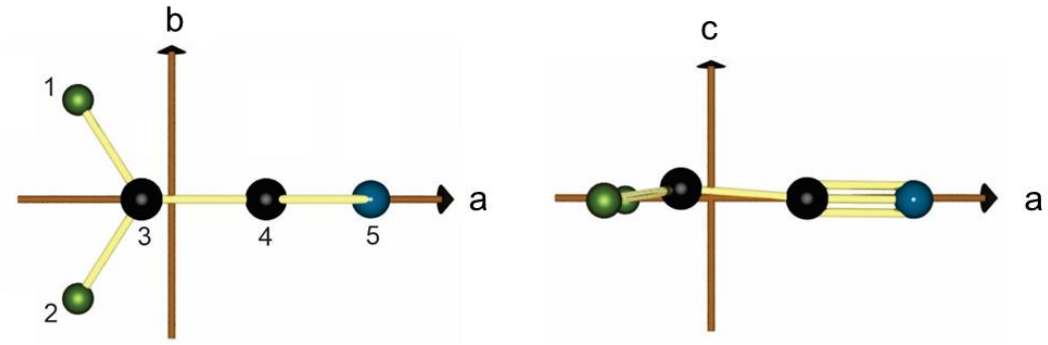

Figure 2. The molecular structure of $\dot{C}F_2CN$ optimized at the uB3LYP/aug-cc-pVQZ level of theory in the *ab* and *ac* principal planes. The fluorine atoms are in light green, carbon atoms grey, and the nitrogen atom is blue. The carbon at the 3 position is referred to as the methylenic carbon in the text. The CN triple bond is shown in the *ac* plane but not visible in profile in the *ab* plane. Upon close inspection, the figures clearly show that the quantum chemical equilibrium geometry is non-planar with a C_s molecular symmetry. The ∠(F,C,F) angle is calculated to be 113°, whereas both ∠(F,C,C) angles are calculated to be 122°.

2.2 . Hamiltonian Models

In open shell molecules, such as doublet molecules, **S** = ½, both fine and hyperfine structures on pure rotational transitions are often observed in highly resolved microwave spectra. The resulting fine and hyperfine parameters that are recoverable from such spectra are of considerable use in understanding a molecule's electronic and geometric structure.

Although the presence of an unpaired electron can introduce three kinds of fine structure interactions, namely spin-orbit, spin-rotation, and spin-spin interactions, in non-linear polyatomic molecules in doublet states the spin-rotation interaction is the most important[38]. The spin-rotation parameters, $\varepsilon_{\alpha\beta}$, are second-order terms often providing insight into the location of excited electronic states.

The **T** tensor represents the through-space anisotropic magnetic dipole - magnetic dipole interaction between the electronic spin **S** and the nuclear spins of the nitrogen nucleus, $\mathbf{I}_{N,}$ and the nuclear spins of the fluorine nuclei, $\mathbf{I}_{F1}$ and $\mathbf{I}_{F2}$. These terms are written as $\mathbf{S}\cdot\mathbf{T}\cdot\mathbf{I}$ and we measured the on-diagonal components of this traceless tensor and one off-diagonal component $\mathbf{T}_{ab}(N)$.

The Fermi contact interaction, a_F, whose Hamiltonian operator is given by $a_F\mathbf{I}\cdot\mathbf{S}$, has no classical analogy. However, we note that Nierenberg has presented a derivation of the Fermi contact term from classical electromagnetic theory [39,40]. The a_F term provides insights into the unpaired electron spin density at the nucleus in question. We measured the Fermi contact term for both the nitrogen, $I_N = 1$, and the fluorine nuclei, $I_{F1} = I_{F2} = ½$.

Finally, nitrogen, with its spin of 1, has a nuclear electric quadrupole tensor interaction between the field gradient of the electrons and the quadrupole moment of the nucleus. We were able to measure all three diagonal elements of the nitrogen nuclear electric quadrupole tensor.

Two quantum number coupling schemes were used in this work to label the quantum states of $\dot{C}F_2CN$. There are two possible symmetry groups, depending on whether the molecule is planar or not. The fluorine nuclei can be treated separately if they can be exchanged by a 180° rotation, going from above to under the C3-C4-N5 plane (see the left-hand side part of Figure 2 for visualization). This requires a C_2 symmetry of the molecule, which in turn requires the molecule to be planar. If $\dot{C}F_2CN$ is not planar, a 180° rotation cannot exchange them (see the right-hand side part of Figure 2), but they are still equivalent since the *ac*-plane is a symmetry/mirror plane. The molecular symmetry is C_s, and the fluorine nuclei cannot be treated separately.

If no assumption about the C_{2v} symmetry of the molecule is made and the nuclear spins of the fluorine atoms are treated independently, a "sequential spin coupling scheme" is used:

$$\mathbf{J} = \mathbf{N} + \mathbf{S}, \qquad \mathbf{F_1} = \mathbf{J} + \mathbf{I}_N, \qquad \mathbf{F}_2 = \mathbf{F_1} + \mathbf{I}_{F1}, \quad \mathbf{F} = \mathbf{F}_2 + \mathbf{I}_{F2}. \tag{1}$$

$\mathbf{I}_{F1}$ and $\mathbf{I}_{F2}$ are the nuclear angular momentum vectors of the two fluorine nuclei, and $\mathbf{I}_N$ is that of the nitrogen nucleus. The Hamiltonian operator can be written as:

$$\mathbf{H} = \mathbf{H}_{rot} + \mathbf{H}_{sr} + \mathbf{H}_{hfs}(N) + \mathbf{H}_{hfs}(F_1) + \mathbf{H}_{hfs}(F_2). \quad (2)$$

Where $\mathbf{H}_{rot}$ is the semi-rigid part consisting of a rigid rotor Hamiltonian supplemented with quartic centrifugal distortion corrections [41]:

$$\mathbf{H}_{\mathrm{rot}} = AN_a^2 + BN_b^2 + CN_c^2 - \Delta_N N^4 - \Delta_{NK}\mathbf{N}^2 N_a^2 - \Delta_K N_a^4 - 2\delta_N \mathbf{N}^2(N_b^2 - N_c^2) - \delta_K\{N_a^2, (N_b^2 - N_c^2)\} \quad (3)$$

and $\mathbf{H}_{sr}$ is the term for the electron spin - molecular overall rotation interactions:

$$\mathbf{H}_{\mathrm{sr}} = \frac{1}{2}\sum_{\alpha\beta} \varepsilon_{\alpha\beta} \left(N_\alpha S_\beta + S_\beta N_\alpha\right). \quad (4)$$

If the off-diagonal terms of the spin-rotation tensor is taken to be zero, Eq. (4) becomes:

$$\mathbf{H}_{\mathrm{sr}} = \varepsilon_{aa} N_a S_a + \varepsilon_{bb} N_b S_b + \varepsilon_{cc} N_c S_c. \quad (5)$$

The last three terms of Eq. (2) contain the magnetic hyperfine interactions between the unpaired electron and the nitrogen and fluorine atoms, as well as the nitrogen quadrupole coupling:

$$\mathbf{H}_{\mathrm{hfs}}(\mathrm{N}) = (a_F)_{\mathrm{N}}\mathbf{S}\cdot\mathbf{I}_{\mathrm{N}} + (T_{aa})_{\mathrm{N}} S_a I_{\mathrm{N}a} + (T_{bb})_{\mathrm{N}} S_b I_{\mathrm{N}b} + (T_{cc})_{\mathrm{N}} S_c I_{\mathrm{N}c} + (T_{ab})_{\mathrm{N}} S_a I_{\mathrm{N}b} + \frac{1}{2I(2I-1)} \sum_{\alpha,\beta} \chi_{\alpha,\beta}\left[I_\alpha, I_\beta\right]_+ \quad (6)$$

$$\mathbf{H}_{\mathrm{hfs}}(\mathrm{F}) = (a_F)_{\mathrm{F1}}\mathbf{S}\cdot\mathbf{I}_{\mathrm{F1}} + (T_{aa})_{\mathrm{F1}} S_a I_{\mathrm{F1}a} + (T_{bb})_{\mathrm{F1}} S_b I_{\mathrm{F1}b} + (T_{cc})_{\mathrm{F1}} S_c I_{\mathrm{F1}c} + (T_{ab})_{\mathrm{F1}} S_a I_{\mathrm{F1}b} + (a_F)_{\mathrm{F2}}\mathbf{S}\cdot\mathbf{I}_{\mathrm{F2}} + (T_{aa})_{\mathrm{F2}} S_a I_{\mathrm{F2}a} + (T_{bb})_{\mathrm{F2}} S_b I_{\mathrm{F2}b} + (T_{cc})_{\mathrm{F2}} S_c I_{\mathrm{F2}c} + (T_{ab})_{\mathrm{F2}} S_a I_{\mathrm{F2}b} \quad (7)$$

where a_F is the Fermi contact term; T_{aa}, T_{bb}, T_{cc}, denote the diagonal terms of the second rank tensors of the magnetic dipolar interaction between **I** and **S**; **S** denotes the electron spin, and $\mathbf{I}_i$ (i = N, F1, F2) denote the nuclear spin corresponding to the i-th nucleus; S_a, S_b, S_c and I_{ia}, I_{ib}, I_{ic} are the components of **S** and $\mathbf{I}_i$ along the principal axis a, b, and c, respectively[38,42,43]. The last term of $\mathbf{H}_{\mathrm{hfs}}(\mathrm{N})$ is the nuclear quadrupole coupling Hamiltonian $\mathbf{H}_Q$ [44], which can be written in a form appropriate for use with Pickett's SPFIT/SPCAT programs[45,46]:

$$\mathbf{H}_Q = \frac{1}{2I(2I-1)}\left\{\frac{3}{2}\chi_{aa}\left[I_a^2 - \frac{1}{3}\mathbf{I}^2\right] + \frac{1}{4}(\chi_{bb} - \chi_{cc})[I_+^2 + I_-^2] + \chi_{ab}[I_aI_b + I_bI_a] + \chi_{ac}[I_aI_c + I_cI_a] + + \chi_{bc}[I_bI_c + I_cI_b]\right\} \quad (8)$$

where the χ_{ij} terms correspond to the components of the nuclear electric quadrupole coupling tensor.

However, if (and only if) $\dot{C}F_2CN$ holds a C_{2v} symmetry like $\dot{C}F_2CCH$, then an alternative spin coupling scheme may be used when there are *n*-equivalent spins. In this case the spins of two fluorine nuclei can couple together to obtain a unique nuclear spin, $\mathbf{I}_F = \mathbf{I}_{F1} + \mathbf{I}_{F2}$, for the fluorine atoms, then couple it with other angular momenta. The so called "$\mathbf{I}_F$ coupling scheme" is given as follows:

$$\mathbf{J} = \mathbf{N} + \mathbf{S}, \qquad \mathbf{F_1} = \mathbf{J} + \mathbf{I}_N, \qquad \mathbf{I}_F = \mathbf{I}_{F1} + \mathbf{I}_{F2}, \quad \mathbf{F} = \mathbf{F_1} + \mathbf{I}_F. \quad (9)$$

For the $\mathbf{I}_F$ coupling scheme, the resulting Hamiltonian is as above with the simplification that $\mathbf{H}_{hfs}(F)$ reduces to:

$$\mathbf{H}_{\text{hfs}}(\text{F}) = (a_F)_\text{F}\mathbf{S}\cdot\mathbf{I}_\text{F} + (T_{aa})_\text{F}S_a\mathbf{I}_{\text{F}_a} + (T_{bb})_\text{F}S_b\mathbf{I}_{\text{F}_b} + (T_{cc})_\text{F}S_c\mathbf{I}_{\text{F}_c} + (T_{ab})_\text{F}S_a\mathbf{I}_{\text{F}_b}. \quad (10)$$

If $\dot{C}F_2CN$ holds a C_{2v} symmetry then the two fluorine atoms can be interchanged by a 180° rotation about the *a*-axis. Therefore, it is meaningful to couple the nuclear spins of ½ of the two fluorine atoms, $\mathbf{I}_F$, to give an ortho nuclear spin triplet state of $\mathbf{I}_F = 1$ (75%) and a para nuclear spin singlet state of $\mathbf{I}_F = 0$ (25%).

Since the two fluorine nuclei are fermions, the total wave function must be anti-symmetric (⊖), that is:

$$\mathbf{\Psi_{tot}} = \mathbf{\Psi_{elec}} \otimes \mathbf{\Psi_{vib}} \otimes \mathbf{\Psi_{rot}} \otimes \mathbf{\Psi_{nucl}(F)} = \ominus. \quad (11)$$

Because the spectra are measured in the electronic and vibrational ground state ($^2B_1$ and v = 0, respectively), the electronic wave function $\mathbf{\Psi_{elec}}$ is ⊖ (negative parity) and the vibrational wave function $\mathbf{\Psi_{vib}}$ is 0^+ (positive parity). Therefore, $\mathbf{\Psi_{rot}} \otimes \mathbf{\Psi_{nucl}(F)} = \oplus$. By exchanging the two fluorine nuclei with an 180° rotation about the *a*-axis, $\mathbf{\Psi_{rot}}$ is ⊖ for K_a odd and ⊕ for K_a even. Finally, the spin wave function for the fluorine nuclear wave function, $\mathbf{\Psi_{nucl}(F)}$, is ⊕ for the ortho state with $\alpha(1)\alpha(2)$, $2^{-½}[\alpha(1)\beta(2) + \beta(1)\alpha(2)]$, $\beta(1)\beta(2)$, and ⊖ for the para state with $2^{-½}[\alpha(1)\beta(2) - \beta(1)\alpha(2)]$. The total wave function can thus only be antisymmetric if the ortho spin state possesses K_a even and the para spin state K_a odd:

$$\Psi_{tot} = \Psi_{elec}^{\ominus} \otimes \Psi_{vib}^{\oplus} \otimes \Psi_{rot}^{\oplus}(K_a \text{ even}) \otimes \Psi_{nucl}^{\oplus}(F)(I_F = 1) = \ominus \quad (12a)$$

$$\Psi_{tot} = \Psi_{elec}^{\ominus} \otimes \Psi_{vib}^{\oplus} \otimes \Psi_{rot}^{\ominus}(K_a \text{ odd}) \otimes \Psi_{nucl}^{\ominus}(F)(I_F = 0) = \ominus \quad (12b)$$

If $\dot{C}F_2CN$ does possess a symmetry axis that passes through the ĊCN atoms and bisects the F–Ċ–F angle then the both the sequential and $\mathbf{I_F}$ coupling schemes should produce similar quality fits to the experimental data with equivalent spectroscopic parameters.

2.3. Experimental

The rotational spectra of $\dot{C}F_2CN$ were recorded using two supersonic jet FTMW spectrometers equipped with pulsed discharge nozzles. A detailed description of the spectrometers can be found elsewhere [47,48]. Many modifications have been made, since the initial construction of the instruments including the coaxial expansion of the gas pulse along the cavity axis for increased sensitivity and resolution, changes in microwave circuitry for decreasing noise, and the software updated for automatic scanning. A gas sample of ~0.3% trifluoracetonitrile CF_3CN seeded in neon or argon carrier gas at a stagnation pressure of ~1 atm is expanded through a 0.8 mm diameter General Valve nozzle. CF_3CN was commercially available (~97%, Matrix Scientific Co.), and used without further purification. The expanding precursor gas pulse encounters a –900 V pulsed discharge that serves to cleave a C–F bond to form the $\dot{C}F_2CN$ radical. The pulsed DC discharge unit [49] is installed right after the General Valve nozzle. The discharge region is ~1 to 2.5 cm away from the nozzle exit. Thereafter, the hot plasma moiety continues to expand until it reaches the Mach disk. The background pressure in the vacuum chamber is ~10^{-6} Torr. The rotational temperature of chemical species in the jet is cooled down to a few Kelvin. At such a low temperature, only the lowest rotational energy levels can be populated. The pulsed plasma jet beam enters the high *Q* Fabry-Pérot cavity, then a microwave pulse is broadcast onto the jet pulse at the center of the cavity. If the transition lies within the 300 kHz bandwidth of the microwave pulse and cavity mode combination, a macroscopic polarization is induced in the molecular species. The free induction decay of this polarization is collected and averaged, usually for a couple hundred gas pulses, then Fourier-transformed to yield the spectrum of $\dot{C}F_2CN$. The full-width-half-maximum (FWHM) of the peak is ~5 kHz, which is comparable to the resolution limit of the spectrometer.

Transitions between 6.5 GHz and 26.5 GHz were measured at Wesleyan University. A preliminary fit was obtained with a root-mean-square (rms) deviation of ~12 kHz, which then allowed higher frequency transitions to be recorded between 26.5 and 38.4 GHz using a Balle-

Flygare FTMW instrument at Harvard University. Helmholtz coils were used to cancel the Earth's magnetic field of ~½ Gauss and ~45° inside the FTMW spectrometer. Using a Gauss meter, adjustments were made until the magnetic field was zero in all directions. A spectrum with and without Helmholtz coils is shown in Figure 3. For a few observed transitions, we found unexpected doublet splittings, with an example illustrated in Figure 3. These observations may arise from an inversion motion which is discussed below. However, these doublets were not considered further in the analyses.

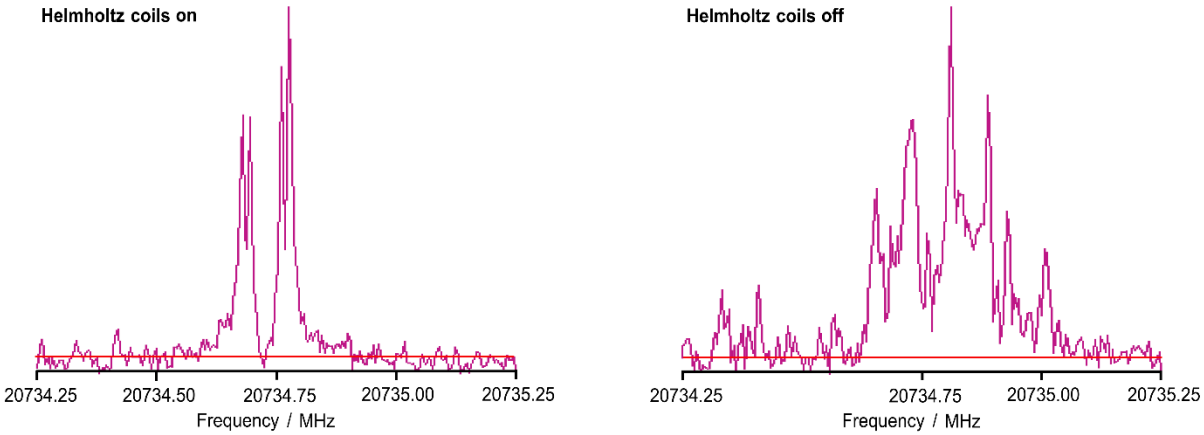

Figure 3. A spectrum of the $3_{03} \leftarrow 2_{02}$ transition of $\dot{C}F_2CN$ with Helmholtz coils turned on (left hand side) and turned off (right hand side).

3. Results and Discussion

3.1. Spectral analysis

Molecular parameters obtained from calculations at the uB3LYP/aug-cc-pVQZ level of theory were sufficiently accurate to give preliminary transition assignments. Therefore, the search for the $\dot{C}F_2CN$ transitions was straightforward. A total of 156 *a*–type rotational transitions, from N = 1 – 0 to 6 – 5 and K_a = 0, 1, 2, 3 were measured and fitted in a global fit using the *SPFIT/SPCAT* program [45] where we applied the sequential spin coupling scheme. A satisfactory standard deviation of 4.0 kHz was achieved for this global fit, which is very close to the experimental accuracy. The spectroscopic parameters obtained are shown in Table 1. The transition frequencies and assignments are given in Table S-2 of the Supplementary Material. The spectroscopic parameters obtained using the $\mathbf{I_F}$ coupling scheme are also shown in Table 1. It is particularly noteworthy that the quality of these fits is significantly worse than that obtained for the sequential coupling scheme and in fact not all the measured lines could be

used in these latter fits. If all the transitions used in the global fit (156) were separated into either $I_F = 0$ transitions (74) and $I_F = 1$ transitions (82) then it was found that the $I_F = 0$ fit produced a microwave rms of 380 kHz well above the line center uncertainties, and the $I_F = 1$ fit would not converge at all. In consequence, and as seen in Table 1, to achieve satisfactory separate $I_F = 0$ and $I_F = 1$ fits, the data sets had to be arbitrarily pruned. This is interpreted as evidence that $\dot{C}F_2CN$ does not hold a C_{2v} symmetry axis along the *a*-axis.

Table 1: Experimental spectroscopic parameters of $\dot{C}F_2CN$ obtained with the program *SPFIT/SPCAT* compared to values predicted at the uB3LYP/aug-cc-pVQZ level of theory.

Par.[a]	**Unit**	**I_F = 0, 1** [b]	**I_F = 0** [c]	**I_F = 1** [c]	**Calc.**[d]
A_0	MHz	11011.074(19)	11010.75(27)	10998.9(48)	11010.2
B_0	MHz	4081.72671(39)	4081.72944(63)	4081.30(17)	4080.5
C_0	MHz	2989.93490(32)	2989.93070(46)	2990.36(17)	2982.5
Δ_N	kHz	0.6011(38)	0.566[e]	0.566[e]	0.566
Δ_{NK}	kHz	18.042(41)	16.3[e]	18.80(32)	16.3
Δ_K	kHz	–1.270[e]	–1.27[e]	–1.27[e]	–1.27
Δ_N	kHz	0.1711(32)	0.160[e]	0.160[e]	0.160
δ_K	kHz	9.700[e]	9.70[e]	9.70[e]	9.70
ε_{aa}	MHz	–46.5629(54)	–46.602(11)	–46.547(32)	/
ε_{bb}	MHz	–23.6850(19)	–23.7199(53)	–23.695(13)	/
ε_{cc}	MHz	–0.12475(89)	–0.1028(27)	–0.1219(91)	/
a_F(N)	MHz	7.9065(21)	7.9116(47)	7.9057(33)	4.49
χ_{aa}(N)	MHz	–4.3780(28)	–4.3735(92)	–4.3983(60)	–4.97
χ_{bb}(N)	MHz	2.8140(45)	2.813(12)	2.882(29)	3.51
χ_{cc}(N)	MHz	1.564(11)	1.561(26)	1.517(80)	1.46
T_{aa}(N)	MHz	–12.1549(30)	–12.1528(47)	–12.1586(61)	–17.9
$(T_{bb}-T_{cc})$(N)	MHz	–32.6189(62)	–32.621(11)	–32.604(52)	–45.7
a_F(F)	MHz	189.163(25)	/	189.189(34)	95.9
T_{aa}(F)	MHz	–178.6635(39)	/	–178.6640(46)	–189
$(T_{bb}-T_{cc})$(F)	MHz	–565.1764(30)	/	–564.83(16)	–600
T_{ab}(F)	MHz	18.723(25)	/	16.69(71)	
N[e]		156	31	65	/
σ[f]	kHz	4.3	4.8	4.6	/

[a] All parameters refer to the principal axis system. Watson's A reduction and I^r representation were used. [b] Global fit including all lines belong to the $I_F = 0$ and 1 states, that is, the sequential coupling scheme. [c] Separate fits performed at the initial assignment stage taking into account either the $I_F = 0$ or 1 state lines, that is, the **I_F** coupling scheme, see text. [d] Ground state

rotational constants and centrifugal distortion constants obtained from anharmonic frequency calculations. [e] Fixed to the calculated value. [e] Number of transitions. [f] Root-mean-squares deviation of the fit.

3.2. Structural Parameters

The ground state rotational constants calculated at the uB3LYP/aug-cc-pVQZ level of theory are in excellent agreement with those deduced from the global *SPFIT/SPCAT* fit. The *A* and *B* constants match almost exactly, and the deviation of 7.4 MHz for the *C* constant is a relative difference of only 0.25%. Although slightly worse for $\dot{C}F_2CCH$, the rotational constants were also quite well predicted at the uB3LYP/aug-cc-pVQZ level [21]. The centrifugal distortion constants agree well with those obtained from the fit. However, the Δ_K and δ_K values were not well-determined and needed to be fixed to the calculated values. The agreement between calculated and observed rotational constants is interpreted to mean that the ground state geometry of $\dot{C}F_2CN$ is not planar as shown in Figure 2.

3.3. Spin-Rotation and Hyperfine Constants

3.3.1. Spin-Rotation Constants

To second order, the expression for the components of the spin-rotation tensor along the molecular principal axes is given by

$$\varepsilon_{\alpha\alpha} = 2\hbar \sum_n \frac{\langle n|L_\alpha/I_{\alpha\alpha}|0\rangle\langle 0|A_{SO}L_\alpha|n\rangle}{E_n - E_0} \qquad (13)$$

where α = *a*, *b*, or *c*, the sum is over the excited electronic states with energy E_n, L_α is the electronic orbital angular momentum operator, $I_{\alpha\alpha}$ are the components of the moment of inertia tensor, and A_{SO} is the spin-orbit coupling constant [38,50,51]. Table 2 shows the spin-rotation parameters, scaled by their respective ground state rotational constants, for a variety of related radicals of the type $\dot{C}X_3$, where X represents either a terminal atom or group (not necessarily the same). We note that the scaled spin-rotation parameters for $\dot{C}F_2CN$, $\dot{C}F_2CCH$, and $\dot{C}H_2F$ are very similar. For the selection of radicals in Table 2, it is readily observed that $|\varepsilon_{aa}/A_0| \approx |\varepsilon_{bb}/B_0| > |\varepsilon_{cc}/C_0|$. From a purely geometric perspective, the relatively small values of ε_{cc}/C_0 are most readily rationalized by noting that for all these radicals, the unpaired electron is in a *p* orbital perpendicular to the "plane" of each molecule such that L_c is close to zero. Notice that $|\varepsilon_{cc}/C_0|$ for $\dot{C}H_3$ (planar) is considerably smaller than for $\dot{C}F_3$ (non-planar). Also, an approximate equality between ε_{aa}/A_0 and ε_{bb}/B_0 may be used as a measure of molecular

planarity where $L_a \approx L_b$. Indeed, the presence of a C_3 symmetry axis requires $L_a = L_b$. However, a thorough comparison is treacherous given that the L_α operator places symmetry requirements on the relevant excited electronic state(s) $| n \rangle$, and it is possible that such excited electronic state symmetries are absent or, at least, of differing energies within a comparative group such as that shown in Table 2.

Table 2. Comparison of the spin-rotation interaction constants for a variety of related radicals. The spin-rotation constants are scaled by the rotational constants and are therefore unitless.

Molecule	Ref	$(\varepsilon_{aa}/A_0) \cdot 10^3$	$(\varepsilon_{bb}/B_0) \cdot 10^3$	$(\varepsilon_{cc}/C_0) \cdot 10^3$
$\dot{C}H_3$	[52]		–1.219(1)	0.02(1)
$\dot{C}H_2F$	[12]	–4.1(1)	–6.003(3)	–0.051(1)
$\dot{C}H_2{}^{35}C$	[14]	–11.4820(4)	–14.900(2)	0.783(2)
$\dot{C}H_2{}^{79}Br$	[17]	–45.898(2)	–61.299(7)	6.258(8)
$\dot{C}H_2I$	[18]	–106.297(1)	–104.145(3)	24.242(3)
$\dot{C}H_2CCH$	[19]	–1.8378(2)	–1.210(3)	–0.056(3)
$\dot{C}H_2CN$	[53]	–2.321(2)	–2.354(7)	–0.206(1)
$\dot{C}F_2CCH$	[21]	–4.2848(8)	–4.478(1)	0.124(1)
$\dot{C}F_2CN$	This work	–4.2288(5)	–5.8027(5)	–0.0417(3)
$\dot{C}F_3$	[54]		–3.348(1)	0.593(1)

3.3.2. Fluorine and Nitrogen Dipolar Coupling Tensors

The dipolar coupling constants of both fluorine and nitrogen atoms in $\dot{C}F_2CN$ are reported in Table 1 and compared with related radicals in Table 3. For both fluorine and nitrogen, it is readily seen that $T_{aa} \approx T_{bb} \approx -\frac{1}{2}T_{cc}$ indicating that at both nuclei the unpaired electron mainly occupies the *p* orbital extending perpendicularly to the molecular plane consistent with the interpretation of the spin-rotation parameters. When the observed T_{cc}(N), 28.386(5) MHz, is compared with the value for atomic nitrogen, 111.04 MHz[55], the *p*-character electron spin density at the nitrogen is calculated to be 20.2%, comparable to the 25.7% spin density at the nitrogen in $\dot{C}H_2CN$. A similar treatment for T_{cc}(F) leads to a spin density on each fluorine atom of 10.6%. A comparison of dipolar couplings and spin densities for related molecules is presented in Table 4. Assuming that the remainder of the spin density is on the methylenic carbon leads to a carbon spin density of 58.6%. The spin densities calculated in this way for the methylenic carbon and fluorine atoms agree well with those determined by a natural atomic orbital (NAO) analysis at the uB3LYP/aug-cc-pVQZ level of theory, which determines the methylenic carbon and fluorine spin densities to be 59% and 7%, respectively. However, the agreement between experimental dipolar coupling and NAO derived nitrogen spin density is

poor with 20.2% and 34%, respectively. This disagreement is likely due to the cyanide carbon itself having an NAO spin density of −12%, that is, an excess of beta electron spin, see Figure 4.

Table 3: Comparison of the hyperfine spectroscopic constants (in MHz) in the $\dot{C}H_2CCH$, $\dot{C}F_2CCH$, $\dot{C}H_2CN$ and $\dot{C}F_2CN$ radicals.

Parameter	**$\dot{C}H_2CCH$**[19]	**$\dot{C}F_2CCH$**[21]	**$\dot{C}H_2CN$**[53]	**$\dot{C}F_2CN$**[a]
Methylenic H/F				
a_F (H/F)	–54.2(1)	145.73(2)	–59.82(30)	189.17(3)
T_{aa} (H/F)	–14.12(2)	−153.502(3)	–15.891(70)	–178.665(4)
T_{bb} (H/F)	12.88(3)	−166.66(3)	10(24)	–193.260(5)
T_{cc} (H/F)	1.25(3)	320.16(3)	–	371.925(6)
T_{ab} (F)		13.4(3)		18.71(2)
Acetylenic H or N				
a_F (H/N)	–36.32(2)	−32.542(4)	9.513(63)	7.907(2)
T_{aa} (H/N)	17.40(2)	16.1589(7)	–15.671(98)	–12.154(3)
T_{bb} (H/N)	–17.22(8)	−16.31(2)	–12.8(13)	–10.233(8)
T_{cc} (H/N)	–0.18(8)	0.0(2)	–	22.387(8)
χ_{aa} (N)			–4.182(98)	–4.3794(28)
χ_{bb} (N)			2.1 (fixed)	2.8131(45)
χ_{cc} (N)			2.082 (fixed)	1.566(11)

[a] This work.

Table 4. Halogen dipolar coupling constants and spin densities on halogen (δ) for a variety of related radicals.

Molecule	Ref	T_{aa} / MHz	T_{bb} / MHz	$-\frac{1}{2}T_{cc}$ / MHz	δ / %[a]
$\dot{C}H_2F$	[12]	–255.205	–212.31	–233.758	13.3
$\dot{C}H_2{}^{35}Cl$	[14]	–32.2968	–23.0041	–27.6505	15.7
$\dot{C}H_2{}^{79}Br$	[17]	–148.38	–109.27	–128.825	15.8
$\dot{C}H_2I$	[18]	–152.964	–138.988	–145.976	18.0
$\dot{C}F_2CCH$	[21]	–153.502	–166.659	–160.081	9.10
$\dot{C}F_2CN$	This work	–178.665	–193.26	–185.963	10.6

[a] Calculated from $T_{cc} / (2 \cdot \frac{2}{5} \cdot P) \cdot 100$ %, where P is the atomic anisotropic hyperfine parameter taken from reference [55].

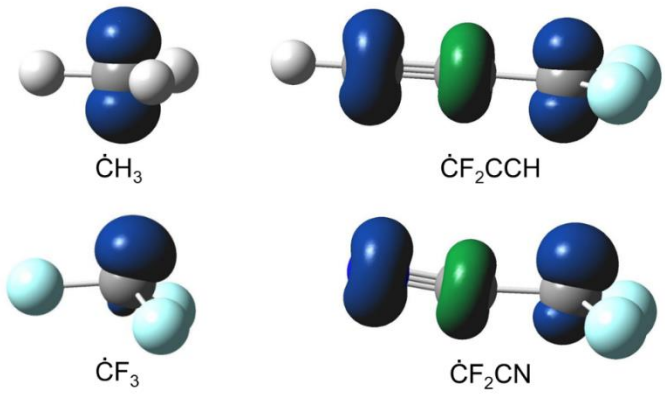

Figure 4. Spin density map of the $\dot{C}H_3$, $\dot{C}F_3$, $\dot{C}F_2CCH$, and $\dot{C}F_2CN$ radicals as calculated by uB3LYP/aug-ccpVQZ. The dark blue and green regions are the α- and β-spin density, respectively.

3.3.3. Fluorine and Nitrogen Isotropic Fermi Contact Terms

Fermi contact terms determined for the fluorine and nitrogen nuclei in $\dot{C}F_2CN$ are presented in Tables 1 and 3. The values obtained are much smaller than the corresponding atomic values and are both positive as expected for heavy atoms. The *s* character of the unpaired electron orbital on the N and F nuclei were both calculated to be 0.4%, where the atomic values for the hyperfine interaction constants were taken from the tables of Morton and Preston [55]. The small *s* character indicates that the unpaired electron occupies almost pure *p* orbitals at both sites. For fluoromethyl radicals, Konishi and Morokuma [56] have provided a relationship between a_F(F) and the bond spin density between the carbon and fluorine, D^{π}_{CF}. The equation is a_F(F) / MHz ≈ –680 D^{π}_{CF}. The term D^{π}_{CF} may be estimated from $-(D^{\pi}_{C}D^{\pi}_{F})^{1/2}$ where D^{π}_{C} and D^{π}_{F} are the p_{π}-orbital spin densities at the carbon and fluorine atoms, respectively. Using D^{π}_{C} = 0.59 and D^{π}_{F} = 0.11 (see above), the equation leads to a_F(F) ≈ 173 MHz in reasonable agreement with the experimental value of 189.17(3) MHz. A simple relationship describing a_F(N) is not available; however, it is notable that a_F(N) in the ĊCN [57], $\dot{C}H_2CN$ [53], and $\dot{C}F_2CN$ radicals are similar at 10.5(11) MHz, 9.51(6) MHz, and 7.907(2) MHz, respectively. As expected, the similar a_F(N) in ĊCN, $\dot{C}H_2CN$, and $\dot{C}F_2CN$ suggests that in all cases the nitrogen atom has similar bonding environments.

3.3.4. Nitrogen Nuclear Quadrupole Coupling Tensor

The nitrogen nuclear quadrupole coupling (NQC) tensor in the molecular principal axes, Table 1, is compared to related nitrogen-containing species NQC tensors in the appropriate quadrupole principal axes systems in Table 5. The quantity $(n_x - n_y) \times 100$ may be taken as the percentage contribution of a $X{=}C{=}N^{(-)}$ type structure to a $X{-}C{\equiv}N$ structure [58] (see Figure 5), where (–) represents a negative formal charge. In Table 6, *p*-orbital populations for a subset of cyanide-containing species, derived from NQC tensors, are compared with quantum mechanically calculated values. The agreement is very good. For $\dot{C}H_2CN$ and $\dot{C}F_2CN$ a structure containing solely $C{=}C{=}N^{(-)}$ would require planarity. It is notable that, of the molecules shown in the table below, $\dot{C}F_2CN$ has the highest contribution of the $C{=}C{=}N^{(-)}$ structure excepting that of CH_2NH, which is planar and contains a "pure" C=N double bond. Also, of the molecules shown in the table below, the bond distance $r(C{\equiv}N) \approx 1.147$ Å for all compounds except for $\dot{C}N$ and $\dot{C}F_2CN$ for which $r(C{\equiv}N) \approx 1.162$ Å, whereas the $r(C{=}N)$ distance in CH_2NH is 1.23 Å. The long CN bond in $\dot{C}F_2CN$ together with a very short $r(C{-}C) = 1.379$ Å are consistent with a structure that has an appreciable contribution of a $C{=}C{=}N^{(-)}$ structure.

Table 5: Nitrogen quadrupole coupling tensors for a selection of related CN-containing molecules.

Molecule	Ref	χ_{zz} / MHz	χ_{yy} / MHz	χ_{xx} / MHz	η[a]	$(n_x - n_y) \cdot 100$[b]
HCN	[59]	–4.7084(11)	2.3542[c]	2.3542[c]	0	0
CF_3CN	[60]	–4.666(4)	2.333[c]	2.333[c]	0	0
CH_3CN	[61]	–4.22473(80)	2.11236(40)	2.11236(40)	0	0
$\dot{C}N$	[62]	–1.275(96)	0.638[c]	0.638[c]	0	0
$\dot{C}CN$	[57]	–4.835(63)	2.418[c]	2.418[c]	0	0
CHF_2CN	[63]	–4.6347(87)	2.3990(90)	2.2357(87)	0.035	0.97
$\dot{C}H_2CN$[d]	[53]	–4.1950(89)	2.362(13)	1.833(13)	0.126	3.15
CH_2FCN	[63]	–4.5278(36)	2.7098(36)	1.8180(40)	0.197	5.31
NF_2CN[e]	[64,65]	–3.90(13)	2.49(13)	1.41(13)	0.277	6.43
$\dot{C}F_2CN$[d]	This work	–4.3794(28)	2.8131(45)	1.566(11)	0.285	7.42
CH_2NH	[66]	–4.51(5)	3.62(1)	0.89(5)	0.605	16.2

[a] The asymmetry of the χ tensor in its principal axes system, $\eta = (\chi_{xx} - \chi_{yy})/\chi_{zz}$.

[b] Calculated from $n_x - n_y = \frac{2}{3}\left(\frac{\chi_{xx}-\chi_{yy}}{eQq_{210}}\right)$ where eQq_{210} = –11.2 MHz [67] and n_x and n_y represent the number of electrons in *p*-orbitals with orientations along the *x* and *y* axes, respectively.

[c] By symmetry.

[d] Off-diagonal terms of the quadrupole coupling tensor in the molecular principal axes system were not determined. The components χ_{aa}, χ_{bb}, χ_{cc} are assumed to map to the nuclear quadrupole principal axes such that $|\chi_{zz}| > |\chi_{yy}| > |\chi_{xx}|$.

[e] The components χ_{xx}, χ_{yy}, χ_{zz} were calculated from χ_{aa}, χ_{bb}, χ_{cc} using a partial r_s-structure.

Table 6. Experimentally derived[a] and calculated[b] numbers of nitrogen unbalanced valence π-electrons, $(U_p)_g$ $g = x, y, z$ and calculated mean number of nitrogen valence π-electrons, N_g, for a selection of related cyanide-containing compounds (see Table 5 for reference of source data).

Molecule	$(U_p)_z$		$(U_p)_y$		$(U_p)_x$		N_z	N_y	N_x
	Expt.	Calc.	Expt.	Calc.	Expt.	Calc.			
CF_3CN	0.447	0.447	–0.223	–0.224	–0.223	–0.224	1.490	1.043	1.043
CHF_2CN	0.444	0.439	–0.230	–0.230	–0.214	–0.209	1.494	1.049	1.063
CH_2FCN	0.433	0.431	–0.259	–0.260	–0.174	–0.171	1.503	1.042	1.101
$\dot{C}F_2CN$	0.419	0.418	–0.269	–0.287	–0.150	–0.131	1.469	0.998	1.103
CH_3CN	0.404	0.415	–0.202	–0.208	–0.202	–0.208	1.513	1.098	1.098
$\dot{C}H_2CN$	0.401	0.414	–0.226	–0.251	–0.175	–0.163	1.485	1.042	1.101

[a] Determined using $(U_p)_z = -\chi_{zz}/eQq_{210}$ etc [58]. A value of eQq_{210} = –10.45 MHz gave the best agreement with calculated values.

[b] From natural atomic orbital analyses at the B3LYP/aug-cc-pVQZ level of theory.

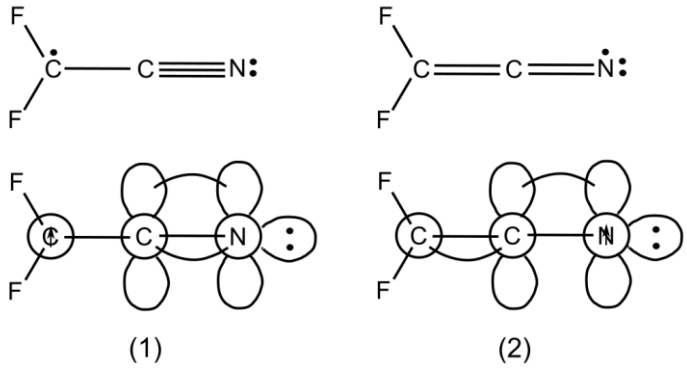

Figure 5. Two resonance structures (1) and (2) of $\dot{C}F_2CN$ illustrating the unpaired electron along the CCN chain. Lines indicate sigma bonding orbitals; π-bonding in-plane *p* orbitals are

drawn in the standard fashion; π-bonding out-of-plane *p* orbitals are drawn as circles for orbitals; arcs indicate π-bonding between the *p* orbitals.

3.4.On the planarity of $\dot{C}F_2CN$

The inertial defect, $\Delta_0 = I_{cc} - I_{aa} - I_{bb} = -2\sum_i m_i c_i^2$, is often used as a measure of planarity. For a rigid, planar molecule, which requires that all *c*-coordinates are zero, then the inertial defect is zero. For a non-planar molecule, the inertial defect is negative. However, it is well known that small negative values of the inertial defect can result for planar molecules with low frequency out of plane vibrations. For $\dot{C}F_2CN$, Δ_0 = –0.686 u$Å^2$, which regarding magnitude, is quite large for a molecule with only 9 normal modes, see Table 7. For comparison, of the planar species presented by Oka [68], the largest magnitude inertial defects are found for styrene and halogenated styrenes for which Δ_0 is between –0.6 and –0.8 u$Å^2$, all of which have many more low-frequency out-of-plane normal modes than $\dot{C}F_2CN$. This result suggests that $\dot{C}F_2CN$ is non-planar in keeping with the B3LYP/aug-cc-pVQZ calculated equilibrium geometry. To explore the source of the "splitting" on several of the observed transitions, a potential function for inversion was calculated at the MP2/cc-pVTZ [69] and B3LYP/cc-pVTZ levels of theory. The potential energy function was obtained by performing a series of geometry optimizations while holding the umbrella angle fixed at values from 0° (planar) to 50° in 2.5-degree steps and then plotting energy versus umbrella angle. The potential energy function obtained in this way is a symmetric double minimum function with the two minima corresponding to mirror images of the molecule reflected through the *ab* principal inertial plane, see Figure 2. Although a formula for the reduced mass of the inversion motion is available for this type of molecule [70], progress was thwarted given the dramatically different inversion potentials obtained from the two levels of theories. At the MP2 level, the barrier to inversion is calculated to be high at 1800 cm^{-1} whereas at the B3LYP level the barrier is very low at just 12 cm^{-1}. The extreme method dependence is interesting and, although providing no insight to the present question, the two reduced potentials are presented in Figure S-1 in the Supplementary Materials.

However, it should be noted that the question of planarity in $\dot{C}F_2CN$ has an extra facet beyond that of a pyramidal methylenic carbon in that the CCN bond is calculated to be 174°, which is visible in Figure 2. Rather than being an artifact of the calculation (lack of convergence, flat potential energy etc.), it is notable that in NF_2CN [71] and PF_2CN [72] the N/P–CN bond has been experimentally determined to be 174° and 171°, respectively. This

suggests that the non-linear CCN bond in $\dot{C}F_2CN$ is likely real. It is interesting to consider the effect of the non-linear CCN bond on the magnitude of the inertial defect. We explored this by first assuming a rigid and planar "CF_2C-" configuration and then adjusted the CCN angle while keeping r(CN) constant to reproduce the experimentally obtained inertial defect of –0.686 uÅ^2. We find that the CCN angle would have to be approximately 165^o to achieve the observed inertial defect, which we believe unreasonable. Secondly, we took the calculated pyramidal structure that matches the observed rotational constants and straightened the CCN angle from 174^o to 180^o. This bond straightening causes the inertial defect to increase in magnitude from –0.686 uÅ^2 to –0.94 uÅ^2. Although these are crude models, the non-linear CCN bond appears to cause the inertial defect to be smaller in the pyramidal configuration which we believe serves as evidence for the non-planar geometry at the methylenic carbon.

Table 7. Experimental inertial defects and predicted lowest frequency out of plane vibrations

Molecule	Ref	Δ_0 / uÅ^2
$\dot{C}H_2F$	[12]	–0.009
$\dot{C}H_2{}^{35}Cl$	[14]	0.0328
$\dot{C}H_2{}^{79}Br$	[16]	0.0322
$\dot{C}H_2I$	[18]	0.0366
$\dot{C}H_2CCH$	[19]	0.0678
$\dot{C}HF_2$	[73]	–0.681
$\dot{C}H_2CN$	[53]	0.0780
$\dot{C}F_2CCH$	[21]	–0.0846
$\dot{C}F_2CN$	This work	–0.686

4. Conclusion

The microwave spectrum of the $\dot{C}F_2CN$ radical was recorded in the frequency range between 6.5 GHz and 38.4 GHz and was assigned using the support of quantum chemical calculations. The fine and hyperfine parameters have allowed us to determine experimental spin densities with the unpaired electron located primarily at the methylenic carbon. Regarding the question whether $\dot{C}F_2CN$ is planar or not, our cautious conclusion is, that $\dot{C}F_2CN$ has a nearly flat pyramidal structure but is not planar. The evidence supporting this conclusion are (i) the agreement between the quantum-chemically calculated and experimental rotational constants; (ii) the relatively large and negative inertial defect deduced from the experimental rotational constants; (iii) the inability to separately fit the $\mathbf{I}_F = 0$ and $\mathbf{I}_F = 1$ spin states, which is consistent with the assumption that the the radical does not have a C_{2v} symmetry.

Acknowledgements

We thank Dr. J. Cheeseman from Gaussian, Inc. for helping us calculate the fine and hyperfine constants. Dr. J. Montgomery, Jr. and Dr. M. Frisch from Gaussian Inc. helped us set up the internal version of the *Gaussian* 03 program package. We thank Dr. M.C. McCarthy and Prof. P. Thaddeus for providing the Harvard spectrometer for the measurements between 26.5 and 38.4 GHz. We also thank Prof. R. Bohn for the constructive comments. This project was supported by National Science Foundation, award number 9423355. H.V.L.N. was supported by the Agence Nationale de la Recherche (ANR, project ID ANR-18-CE29-0011). T.A.B is with the Pacific Northwest National Laboratory. PNNL is a multiprogram national laboratory operated for the U.S. Department of Energy by Battelle Memorial Institute under Contract DE-AC05-76RL01830. S.A.C. acknowledges financial support from Purchase College SUNY via the Taina Chao Fellowship.

References

[1] G. Herzberg, J. Shoosmith, Canadian Journal of Physics 34 (1956) 523–525.

[2] G. Herzberg, Proceedings of the Royal Society of London. Series A. Mathematical and Physical Sciences 262 (1961) 291–317.

[3] T. Cole, H.O. Pritchard, N.R. Davidson, H.M. McConnell, Molecular Physics 1 (1958) 406–409.

[4] M. Karplus, The Journal of Chemical Physics 30 (1959) 15–18.

[5] R.W. Fessenden, R.H. Schuler, The Journal of Chemical Physics 43 (1965) 2704–2712.

[6] G.A. Carlson, G.C. Pimentel, The Journal of Chemical Physics 44 (1966) 4053–4054.

[7] D.E. Milligan, M.E. Jacox, J.J. Comeford, The Journal of Chemical Physics 44 (1966) 4058–4059.

[8] C. Lifshitz, W.A. Chupka, The Journal of Chemical Physics 47 (1967) 3439–3443.

[9] K. Morokuma, L. Pedersen, M. Karplus, The Journal of Chemical Physics 48 (1968) 4801–4802.

[10] L. Pauling, The Journal of Chemical Physics 51 (1969) 2767–2769.

[11] F. Bernardi, W. Cherry, S. Shaik, N.D. Epiotis, Journal of the American Chemical Society 100 (1978) 1352–1356.

[12] Y. Endo, C. Yamada, S. Saito, E. Hirota, The Journal of Chemical Physics 79 (1983) 1605–1611.

[13] Y. Endo, S. Saito, E. Hirota, Canadian Journal of Physics 62 (1984) 1347–1360.

[14] S. Bailleux, P. Dréan, Z. Zelinger, M. Godon, Journal of Molecular Spectroscopy 229 (2005) 140–144.

[15] S. Bailleux, P. Dréan, M. Godon, Z. Zelinger, C. Duan, Phys. Chem. Chem. Phys. 6 (2004) 3049–3051.

[16] S. Bailleux, P. Dréan, Z. Zelinger, S. Civiš, H. Ozeki, S. Saito, The Journal of Chemical Physics 122 (2005) 134302.

[17] H. Ozeki, T. Okabayashi, M. Tanimoto, S. Saito, S. Bailleux, The Journal of Chemical Physics 127 (2007) 224301.

[18] S. Bailleux, P. Kania, J. Skřínský, T. Okabayashi, M. Tanimoto, S. Matsumoto, H. Ozeki, The Journal of Physical Chemistry A 114 (2010) 4776–4784.

[19] K. Tanaka, Y. Sumiyoshi, Y. Ohshima, Y. Endo, K. Kawaguchi, The Journal of Chemical Physics 107 (1997) 2728–2733.

[20] S. Saito, S. Yamamoto, The Journal of Chemical Physics 107 (1997) 1732–1739.

[21] L. Kang, S.E. Novick, The Journal of Chemical Physics 125 (2006) 054309.

[22] L. Birckenbach, K. Kellermann, Berichte Der Deutschen Chemischen Gesellschaft (A and B Series) 58 (1925) 786–794.

[23] M.J. Molina, F.S. Rowland, Nature 249 (1974) 810–812.

[24] A. McCulloch, Journal of Fluorine Chemistry 123 (2003) 21–29.

[25] S. Solomon, J. Alcamo, A.R. Ravishankara, Nature Communications 11 (2020) 4272.

[26] M. Lickley, S. Fletcher, M. Rigby, S. Solomon, Nature Communications 12 (2021) 2920.

[27] Y. Zhao, Y. Kondo, F.J. Murcray, X. Liu, M. Koike, H. Irie, K. Strong, K. Suzuki, M. Sera, Y. Ikegami, Geophysical Research Letters 27 (2000) 2085–2088.

[28] E. Jaszczak, Ż. Polkowska, S. Narkowicz, J. Namieśnik, Environmental Science and Pollution Research 24 (2017) 15929–15948.

[29] J.B. Burkholder, R.A. Cox, A.R. Ravishankara, Chemical Reviews 115 (2015) 3704–3759.

[30] S. v. Levchenko, A.I. Krylov, The Journal of Physical Chemistry A 106 (2002) 5169–5176.

[31] A.D. Becke, The Journal of Chemical Physics 98 (1993) 5648–5652.

[32] C. Lee, W. Yang, R.G. Parr, Physical Review B 37 (1988) 785–789.

[33] E.F.C. Byrd, C.D. Sherrill, M. Head-Gordon, The Journal of Physical Chemistry A 105 (2001) 9736–9747.

[34] R.D. Cohen, C.D. Sherrill, The Journal of Chemical Physics 114 (2001) 8257–8269.

[35] M.O. Sinnokrot, C.D. Sherrill, The Journal of Chemical Physics 115 (2001) 2439–2448.

[36] M.J. Frisch, G.W. Trucks, H.B. Schlegel, G.E. Scuseria, M.A. Robb, J.R. Cheeseman, J.A. Montgomery Jr., T. Vreven, K.N. Kudin, J.C. Burant, J.M. Millam, S.S. Iyengar, J. Tomasi, V. Barone, B. Mennucci, M. Cossi, G. Scalmani, N. Rega, G.A. Petersson, H. Nakatsuji, M. Hada, M. Ehara, K. Toyota, R. Fukuda, J. Hasegawa, M. Ishida, T. Nakajima, Y. Honda, O. Kitao, H. Nakai, M. Klene, X. Li, J.E. Knox, H.P. Hratchian, J.B. Cross, V. Bakken, C. Adamo, J. Jaramillo, R. Gomperts, R.E. Stratmann, O. Yazyev, A.J. Austin, R. Cammi, C. Pomelli, J.W. Ochterski, P.Y. Ayala, K. Morokuma, G.A. Voth, P. Salvador, J.J. Dannenberg, V.G. Zakrzewski, S. Dapprich, A.D. Daniels, M.C. Strain, O. Farkas, D.K. Malick, A.D. Rabuck, K. Raghavachari, J.B. Foresman, J. v Ortiz, Q. Cui, A.G. Baboul, S. Clifford, J. Cioslowski, B.B. Stefanov, G. Liu, A. Liashenko, P. Piskorz, I. Komaromi, R.L. Martin, D.J. Fox, T. Keith, M.A. Al-Laham, C.Y. Peng, A. Nanayakkara, M. Challacombe, P.M.W. Gill, B. Johnson, W. Chen, M.W. Wong, C. Gonzalez, J.A. Pople, (n.d.).

[37] M.J. Frisch, G.W. Trucks, H.B. Schlegel, G.E. Scuseria, M.A. Robb, J.R. Cheeseman, G. Scalmani, V. Barone, G.A. Petersson, H. Nakatsuji, X. Li, M. Caricato, A. v

Marenich, J. Bloino, B.G. Janesko, R. Gomperts, B. Mennucci, H.P. Hratchian, J. v Ortiz, A.F. Izmaylov, J.L. Sonnenberg, D. Williams-Young, F. Ding, F. Lipparini, F. Egidi, J. Goings, B. Peng, A. Petrone, T. Henderson, D. Ranasinghe, V.G. Zakrzewski, J. Gao, N. Rega, G. Zheng, W. Liang, M. Hada, M. Ehara, K. Toyota, R. Fukuda, J. Hasegawa, M. Ishida, T. Nakajima, Y. Honda, O. Kitao, H. Nakai, T. Vreven, K. Throssell, J.A. Montgomery Jr., J.E. Peralta, F. Ogliaro, M.J. Bearpark, J.J. Heyd, E.N. Brothers, K.N. Kudin, V.N. Staroverov, T.A. Keith, R. Kobayashi, J. Normand, K. Raghavachari, A.P. Rendell, J.C. Burant, S.S. Iyengar, J. Tomasi, M. Cossi, J.M. Millam, M. Klene, C. Adamo, R. Cammi, J.W. Ochterski, R.L. Martin, K. Morokuma, O. Farkas, J.B. Foresman, D.J. Fox, (2016).

[38] E. Hirota, High-Resolution Spectroscopy of Transient Molecules, Springer Berlin Heidelberg, Berlin, Heidelberg, 1985.

[39] W.A. Nierenberg, Annual Review of Nuclear Science 7 (1957) 349–406.

[40] H. Hameka, Advanced Quantum Chemistry: Theory of Interactions between Molecules and Electromagnetic Fields, Addison-Wesley Publishing Company, Reading, Mass., 1965.

[41] J.K.G. Watson, in: J.R. Durig (Ed.), Vibrational Spectra and Structure, Eslevier Scientific Publishing Company, 1977.

[42] I.C. Bowater, J.M. Brown, Carrington Alan, Proceedings of the Royal Society of London. A. Mathematical and Physical Sciences 333 (1973) 265–288.

[43] A. Carrington, Microwave Spectroscopy of Free Radicals, Academic Press, 1974.

[44] E. Hirota, J.M. Brown, J.T. Hougen, T. Shida, N. Hirota, Pure and Applied Chemistry 66 (1994) 571–576.

[45] H.M. Pickett, Journal of Molecular Spectroscopy 148 (1991) 371–377.

[46] S.E. Novick, Journal of Molecular Spectroscopy 329 (2016) 1–7.

[47] A.R.H. Walker, W. Chen, S.E. Novick, B.D. Bean, M.D. Marshall, The Journal of Chemical Physics 102 (1995) 7298–7305.

[48] M.C. McCarthy, M.J. Travers, A. Kovacs, C.A. Gottlieb, P. Thaddeus, The Astrophysical Journal Supplement Series 113 (1997) 105–120.

[49] W. Chen, S.E. Novick, M.C. McCarthy, C.A. Gottlieb, P. Thaddeus, The Journal of Chemical Physics 103 (1995) 7828–7833.

[50] R.F. Curl, Molecular Physics 9 (1965) 585–597.

[51] J.M. Brown, T.J. Sears, J.K.G. Watson, Molecular Physics 41 (1980) 173–182.

[52] C. Yamada, E. Hirota, K. Kawaguchi, The Journal of Chemical Physics 75 (1981) 5256–5264.

[53] H. Ozeki, T. Hirao, S. Saito, S. Yamamoto, The Astrophysical Journal 617 (2004) 680–684.

[54] Y. Endo, C. Yamada, S. Saito, E. Hirota, The Journal of Chemical Physics 77 (1982) 3376–3382.

[55] J.R. Morton, K.F. Preston, Journal of Magnetic Resonance (1969) 30 (1978) 577–582.

[56] H. Konishi, K. Morokuma, Journal of the American Chemical Society 94 (1972) 5603–5612.

[57] J.K. Anderson, D.T. Halfen, L.M. Ziurys, Journal of Molecular Spectroscopy 307 (2015) 1–5.

[58] W. Gordy, R.L. Cook, Microwave Molecular Spectra, 3rd ed., John Wiley & Sons, 1984.

[59] H.A. Bechtel, A.H. Steeves, B.M. Wong, R.W. Field, Angewandte Chemie International Edition 47 (2008) 2969–2972.

[60] A.P. Cox, M.C. Ellis, A.C. Legon, A. Wallwork, J. Chem. Soc., Faraday Trans. 89 (1993) 2937–2944.

[61] G. Cazzoli, C. Puzzarini, Journal of Molecular Spectroscopy 240 (2006) 153–163.

[62] E. Klisch, T. Klaus, S.P. Belov, G. Winnewisser, E. Herbst, Astronomy and Astrophysics 304 (1995) L5.

[63] W. Kasten, H. Dreizler, B.E. Job, J. Sheridan, Zeitschrift Für Naturforschung A 38 (1983) 1015–1021.

[64] M. Winnewisser, F. Stroh, Journal of Molecular Structure 190 (1988) 357–376.

[65] W.C. Bailey, Http://Nqcc.Wcbailey.Net/ (n.d.).

[66] L. Dore, L. Bizzocchi, C. Degli Esposti, J. Gauss, Journal of Molecular Spectroscopy 263 (2010) 44–50.

[67] A. Schirmacher, H. Winter, Physical Review A 47 (1993) 4891–4907.

[68] T. Oka, Journal of Molecular Structure 352–353 (1995) 225–233.

[69] Chr. Møller, M.S. Plesset, Physical Review 46 (1934) 618–622.

[70] J.K. Tyler, J. Sheridan, C.C. Costain, Journal of Molecular Spectroscopy 43 (1972) 248–261.

[71] P.L. Lee, K. Cohn, R.H. Schwendeman, Inorganic Chemistry 11 (1972) 1920–1923.

[72] P.L. Lee, K. Cohn, R.H. Schwendeman, Inorganic Chemistry 11 (1972) 1917–1920.

[73] N. Inada, K. Saito, M. Hayashi, H. Ozeki, S. Saito, Chemical Physics Letters 284 (1998) 142–146.